Elastically modulated wavy vortex flow

Theofilos Boulafentis, Tom Lacassagne, Neil Cagney, Stavroula Balabani

Journal of Non-Newtonian Fluid Mechanics 330 (2024) 105283

Contents lists available at ScienceDirect

Journal of Non-Newtonian Fluid Mechanics

journal homepage: www.elsevier.com/locate/jnnfm

Elastically modulated wavy vortex flow

T. Boulafentis [a], T. Lacassagne [b], N. Cagney [c], S. Balabani [a,*]

[a] Department of Mechanical Engineering, University College London, WC1E 6BT, UK
[b] IMT Nord Europe, Institut Mines-Télécom, Univ. Lille, Centre for Energy and Environment, Lille, F-59000, France
[c] School of Engineering and Materials Science, Queen Mary University of London, E1 4NS, UK

ARTICLE INFO

Keywords:
Taylor-couette flow
Polymers
Viscoelasticity
Absolute/convective instability

ABSTRACT

We investigate the transition pathway of low elasticity fluids ($El = 0.003 - 0.008$) in a Taylor-Couette configuration using low-molecular-weight polyacrylamide (PAAM) and visualisation experiments in the Reynolds range from 0 to 300. We report here for the first time an elastically modified wavy vortex flow state with altered spectral and structural characteristics, that precedes the onset of the traditional (inelastic) Newtonian wavy instability. This new wavy regime is characterised by oscillations of both the inflow and outflow boundaries, associated with a weakening of the outflow regions due to low hoop stresses. The modification of the boundaries persists at higher Reynolds numbers, where the spectral characteristics are unaltered compared to the inelastic, Newtonian case. In addition, a hysteretic behaviour is observed for increasing elasticity, as instabilities are shifted towards lower critical Reynolds numbers, confirming the importance of even vanishing elasticity on the stability of Taylor-Couette flows. At higher fluid elasticity ($El = 0.06$), the amplitude of inflows/outflows oscillations increases, and momentum is transferred axially between adjacent vortices, which may contribute to the emergence of Rotating Standing Waves.

1. Introduction

The instabilities of Newtonian fluids subjected to shear between two concentric cylinders, with one or both rotating, namely Taylor-Couette flow (TCF), have been well-documented [17,22,24]. The most commonly used control parameter for these instabilities in the simplest case of a stationary outer and rotating inner cylinder is the Reynolds number, $Re = \rho\Omega_i r_i d/\eta$, where ρ is the fluid density, Ω_i is the rotational speed of the inner cylinder, r_i is the radius of the inner cylinder, d is the gap between the two cylinders, η is the dynamic shear viscosity of the fluid. The primary instability leads to the formation of equally-spaced, axisymmetric vortices, termed Taylor Vortex Flow (TVF), named after the pioneering work of Taylor [42]. With increasing inertia, such secondary flows undergo a transition into non-axisymmetric, axially oscillating vortices, a regime termed Wavy Vortex Flow (WVF). WVF has been studied for a wide range of geometrical parameters, both analytically and experimentally; an abundance of wave modes have been revealed, attributed to an azimuthally moving wave whose speed depends on Re [2,28,47]. A second travelling wave emerges as Re increases further, leading to a quasi-periodic instability termed Modulated Wavy Vortex Flow (MWVF) [13,27,40,41], prior to the appearance of the so-called broadband spectral component, signifying the onset of chaos [22]. The wavy and modulated wavy instabilities are associated with enhanced intercellular mixing compared to TVF due to the presence of the azimuthal wave which distorts the vortices periodically, allowing intervortex momentum transfer [1,16].

Viscoelasticity, induced by the addition of polymer chains, modulates the aforementioned Newtonian TCF sequence, leading to a variety of more complex transition pathways that depend on the Elasticity Number, $El = t_e\eta/\rho d^2$, where t_e is the relaxation time. Most studies in the literature, focus on the transitions of solutions with Elasticity numbers in the range $El = 0.023 - 27$ which are highly unstable [6,44] and are characterised by the appearance of distinct flow states like Rotating Standing Waves (RSW), Ribbons (RB) and Flame Pattern (FP) [7,32,39].

However, in the limit of vanishing elasticities ($El \sim 0$), published literature reports Newtonian-like transitions in dilute solutions of long-chained polymers or solutions with high polymer entanglement, which most of the time also exhibit shear-thinning behaviour ([9–11]; [14,18]). Yet, some observations, such as the high-frequency WVF with reduced amplitude oscillations in [14], suggest that even in cases where the transition appears Newtonian-like, the flow instabilities can be modified by the smallest amount of elasticity. Performing long

* Corresponding author.
E-mail address: s.balabani@ucl.ac.uk (S. Balabani).

https://doi.org/10.1016/j.jnnfm.2024.105283
Received 12 January 2024; Received in revised form 1 May 2024; Accepted 1 July 2024
Available online 2 July 2024

experiments in the presence of low-molecular-weight polyacrylamide (PAAM) at a constant imposed shear rate, [36] have reported a modification of time-dependent Newtonian flows leading to oscillations at the boundaries with varying amplitude, which were eventually dampened after 20 h. Surprisingly, this was not the case after decreasing the rotational speed of the inner cylinder, indicating a dependence of the flow on the shear history. Dutcher and Muller [18] reported a similar example of altered time-dependent flows, where a MWVF flow state was interposed for a short *Re* range between two WVF regimes in the transition path. Surprisingly, this was accompanied by a delay on the onset of TVF as the elasticity increased, also reported in [10,14,46], possibly attributed to shear-thinning effects. At high *Re*, around $Re \cong 800$, well-above the Newtonian WVF stability limit and after the appearance of MWVF, a flow state reminiscent to WVF with altered structural characteristics appeared [18].

The presence of fluid shear-thinning in experimental [9,19,48,20] and numerical [45,48] studies makes it difficult to disentangle the effects of elasticity and shear-thinning on observed transitions and flow phenomena.

Nevertheless, the experimental studies outlined above indicate a strong effect of even low elasticities on time-dependent and weakly turbulent flow states, but it remains unclear how the flow transitions are affected in the case of vanishingly small elasticity.

In this work, experiments with low molecular weight polyacrylamide (PAAM) polymer solutions were performed, with the following two objectives: firstly, to refine our understanding of elastic instabilities in the case of vanishing elasticities and absence of shear-thinning-achieved through short-chained polymers- for increasing or decreasing inertia; secondly to ascertain whether the increasing entanglement of polymer chains is sufficient to trigger higher-order instabilities like the RSW/FP. To this end, an experiment with a higher elasticity fluid, i.e. using longer chain polymers, has also been performed to link RSW to the Newtonian-like, wavy instabilities.

2. Materials and methods

We employ the same TC geometry (Fig. 1) as in our previous work [11,29,29,31]. It has a height of $H = 135$ mm, inner and outer cylinders radii of $r_i = 21.66$ mm and $r_o = 27.92$ mm, respectively, resulting in a gap width of $d = 6.26$ mm, an aspect ratio of $\Gamma = H/d = 21.56$, a radius ratio of $\eta_{cell} = r_i/r_o = 0.776$ and a curvature of $d/r_i = 0.289$. The TC was placed in a recirculating water tank to maintain the fluid temperature constant throughout the experiments at 20 ± 0.1°C. Both the TC cell and the outer water container are made of transparent material for optical flow measurements. The inner cylinder was rotated by means of a stepper motor (SmartDrive Ltd, Cambridge, UK), with micro-stepping function of 52,000 microsteps/revolution as described in [29,31].

A highly viscous solvent of 72 % glycerol/water (WGL-72) and a low-molecular-weight ($M_n = 20,000\ \mathrm{g\cdot mol^{-1}}$) PAAM polymer were selected to introduce low values of elasticities and negligible shear-thinning. Polymer solutions with concentrations varying in the range of 500–7000 ppm were prepared and their shear rheology was measured in an ARES rheometer at 20 °C, using a Couette geometry with r_i=32 mm and r_o=34 mm. The resulting shear viscosity curves are illustrated in

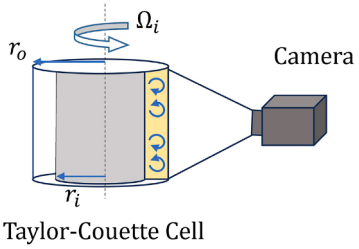

Fig. 1. The Taylor-Couette cell and visualisation setup used in this work.

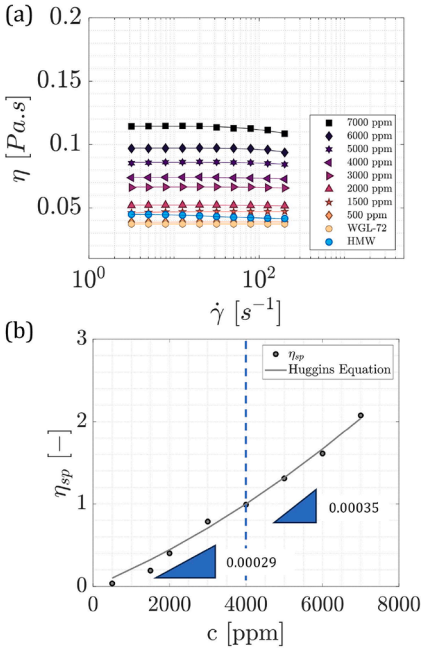

Fig. 2. (a) Viscosity curves for polymer solutions of low-molecular-weight PAAM. The solvent case is noted as WGL-72 and the high-molecular-weight PAAM solution as HMW. All solutions have almost constant viscosity and can be considered Boger fluids. (b) Fitting of Huggins equation to the specific viscosity data, $\eta_{sp} = (\eta_0 - \eta_s)/\eta_s$, where η_0 is the zero-shear viscosity and η_s the solvent viscosity.

Fig. 2a. All solutions exhibit almost constant viscosity for the range of shear rates studied and thus can be considered Boger fluids. This can be quantified using the average scaling exponent of shear stress with strain rate, $\overline{n_e}$, which tends to unity for Boger fluids (Table 1). By fitting the Huggins equation [8] in the viscosity data (Fig. 2b), the critical overlap concentration (i.e. the polymer concentration above which polymer chains entanglement becomes significant) was estimated to be $c^* = 3967$ ppm ($[\eta] = 0.0002$, $k_H = 0.3695$).

An additional solution was prepared with the same solvent using 200 ppm of high-molecular-weight PAAM ($M_w = 5.5 \times 10^6\ \mathrm{g\cdot mol^{-1}}$), to achieve higher fluid elasticity. The viscosity curve of this solution is noted as HMW in Fig. 2a. This solution lies also in the dilute regime ($c^* = 718$ ppm) (the analysis for the estimation of c^* for this polymer is not shown here for brevity).

Among all the fluids characterized in Fig. 2, two polymer concentrations corresponding to the dilute and a semi-dilute regime (1500 ppm and 5000 ppm, respectively) were employed in the present TC experiments, alongside the pure solvent case (WGL-72, Newtonian inelastic) and the HMW solution. The relaxation time of the two low-molecular-weight polymer solutions was estimated using extensional rheology implementing the Slow Retraction Method (SRM) [12,38] and was found equal to $t_e = 2.4$ and 4.4 ms for the 1500 and 5000 ppm, respectively, corresponding to $El = 0.003$ and 0.008. The

Table 1
Rheological characteristics of the solutions used in the TC experiments.

Solution	State	η [Pa.s]	$\overline{n_e}$	t_e [ms]	$\beta = \eta_p/\eta_0$	El
Newtonian						
WGL-72	–	0.0372	1	–	–	–
Low molecular weight polymer						
1500 ppm	Dilute	0.0469	1	2.4	0.261	0.003
5000 ppm	Semi-dilute	0.0856	0.997	4.4	1.3	0.008
High molecular weight polymer						
HMW	Dilute	0.0436	0.987	65.6	0.172	0.06

high-molecular-weight solution relaxation time was estimated using the same method at $t_e = 65.6$ ms, resulting in $El = 0.06$. All fluid properties used in the TC experiments are summarised in Table 1.

Experiments for the low-molecular-weight solutions were performed for (a) increasing Re (ramp-up) (b) decreasing Re (ramp-down) and (c) fixed Re (steady-states). Measurements covered the range $Re = 0 - 300$. Polymer degradation was considered unlikely for the short-chained polymers used in this work. The absence of degradation was further validated by repeating a ramp-up experiment to ascertain that the transitional sequence remains unaltered. The inner cylinder was accelerated/decelerated sufficiently slowly to ensure quasi-static ramp-up/down conditions. The non-dimensional acceleration Γ_0, which takes into account the variation of Re compared to the viscous time scale, was kept well-bellow the quasi-static limit, $\Gamma_0 = 0.3 < 1$ [11,17,29,30](Table 2). For the high-molecular-weight solution, a steady-state experiment at $Re = 105$ was performed.

The Taylor-Couette flow was visualized using mica flakes (10–100 μm, Cornelissen & Son, Pearl Lustre Pigments), added to the solution before each experiment [5,11,29] at low enough volume fraction (0.01% v/v) to not affect the rheological properties of the fluids [23]. A flow strip along the height of the cell (2176 × 16 pixels) was imaged using a high-speed camera (Phantom Miro M340, Vision Research). The acquisition frequency was $f_s = 80$ Hz for the Newtonian case and $f_s = 130$ Hz and 180 Hz for $El = 0.003$ and $El = 0.008$, respectively. More than 300 frames/Re ($1/\Delta Re > 300$), were acquired in all cases (Table 2), where ΔRe is the variation of Reynolds number between two consecutive frames. A much higher acquisition frequency of $f_s = 2000$ Hz was selected for the steady-state experiments to provide high temporal resolution of the wavy and RSW flows.

Following the acquisition, the image intensity was averaged to obtain a single column of intensity I values, and spatiotemporal maps $I(z,t)$ were assembled by stacking different time points horizontally (where z- and t- axes indicate spatial and temporal dimensions, respectively). The intensity was then inverted to highlight the inflows/outflow boundaries. In the ramp-up/down experiments, the t-axis was converted to Re. Fast Fourier Transform was applied on the spatiotemporal intensity maps, both temporally (along the t-axis) and spatially (along the z-axis), to reveal the dominant frequencies and wavelengths of the flow, respectively. Frequency maps were thus constructed by separating the ramp-up/down maps into sections with 512 columns and 50 % overlap, as described in [29].

3. Results and discussion

The transition sequence for the solvent case (not shown here for brevity) is non-hysteretic (i.e. the same transition sequence occurs for ramp-up and ramp-down) and well documented in the literature [3,17,47]. Namely, the laminar Couette flow transitions firstly into TVF at $Re^{ru}_{TVF} = 100$ and secondly to WVF at $Re^{ru}_{WVF} = 200$, where the subscript signifies the flow state at which the flow transitions and the superscript either the ramp-up or ramp-down. No transition to MWVF was observed in the range of Re studied here. The axial wavelength of the flow remains the same for both TVF and WVF and was found equal to $\lambda = 1.7d$ (Fig. 3b). The wavy frequency in the WVF scales linearly with the rotational frequency of the inner cylinder, $f = 1.3 f_i$, where $f_i = \Omega_i/2\pi$.

The dilute low molecular weight polymer mixture (1500 ppm) has an elasticity value $El = 0.003$ and exhibits a transition sequence during the ramp-up that closely resembles the Newtonian case (Fig. 4a). The critical Reynolds numbers for the transition to TVF and WVF remain unaffected ($Re^{ru}_{TVF} = 100$ and $Re^{ru}_{WVF} = 200$). However, just before the appearance of WVF, a non-axisymmetric instability is observed for a small range of Reynolds numbers $Re = 158 - 200$, as evidenced by a distinct ridge on the frequency maps (Fig. 4c, d). This instability has the same wavelength (Fig. 3b) as TVF and WVF but occurs at a lower frequency compared to WVF (Fig. 3a). The wave frequency is not directly proportional to the cylinder oscillation frequency, with $f = 1.15 f_i$ at the onset of the instability ($Re^{ru}_{EWVF} = 158$) and $f = 1.08 f_i$ at the transition to WVF ($Re^{ru}_{WVF} = 200$). Within this range the frequency increases linearly.

We term this low-frequency instability Elastic Wavy Vortex Flow (EWVF) and to the best of our knowledge, it has not been reported previously. Elastic modifications of WTV flows have been reported by a number of researchers. For example, Crumeyrolle et al. [14] observed

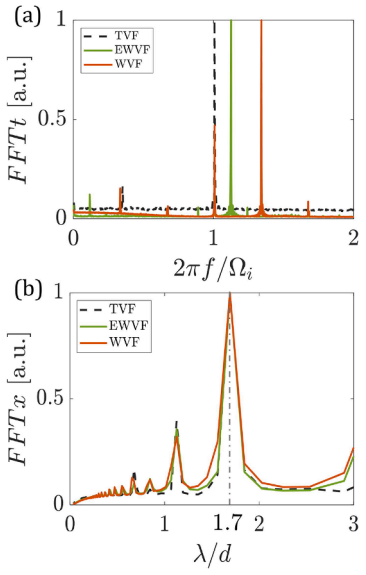

Fig. 3. (a) Temporal and (b) spatial spectra for the inelastic case $El = 0$ ($Re = 180$ - TVF) and $El = 0.003$ ($Re = 180$ - EWVF, $Re = 250$ - WVF). TVF, EWVF, WVF have the same spatial wavelength but different temporal characteristics.

Table 2
Experimental settings for ramp-up/down and steady-state experiments presented later in the results section.

Solution	Experiment Type	Reynolds Range	f_s [Hz]	$1/\Delta Re$	Ω_{max} [s^{-1}]	$d\Omega/dt$ [s^{-2}]	Γ_0
Newtonian							
WGL-72	RU/RD	0 – 300	80	336.54	68.7	0.054	0.3
WGL-72	Steady-State	180	2000	–	34.35	–	–
WGL-72	Steady-State	250	2000	–	60	–	–
Low molecular weight polymer							
1500 ppm	RU/RD	0–300	130	351.6	90.42	0.0943	0.3
5000 ppm	RU/RD	0–300	180	317.84	163.67	0.309	0.3
1500 ppm	Steady-State	180	2000	–	54.29	–	–
1500 ppm	Steady-State	250	2000	–	75.33	–	–
5000 ppm	Steady-State	180	2000	–	98.2	–	–
5000 ppm	Steady-State	250	2000	–	136.4	–	–
High molecular weight polymer							
HMW (200 ppm)	Steady-State	105	2000	–	26.05	–	–

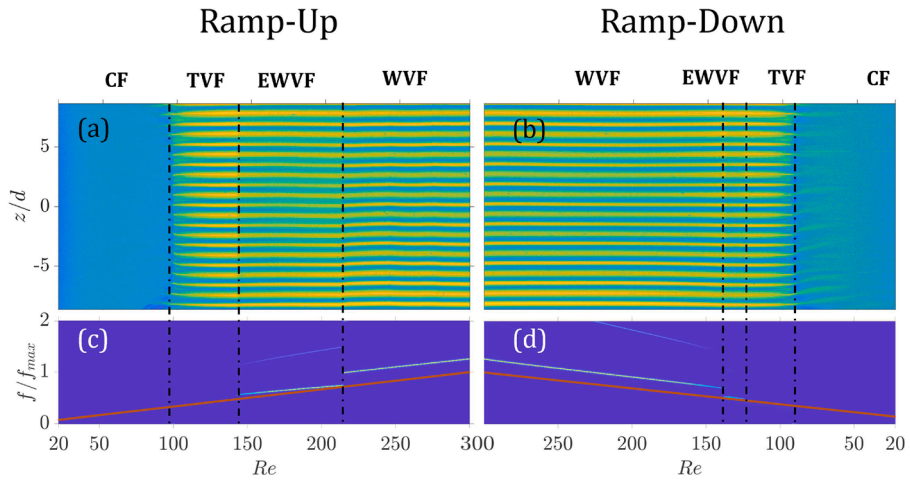

Fig. 4. Spatiotemporal maps for ramp-up (a) and ramp-down (b) experiments and corresponding frequency maps (c) and (d) for $El = 0.003$. The orange line in the frequency maps (c), (d) denotes the rotational frequency. f_{max} in (c) and (d) corresponds to the maximum rotational speed of the inner cylinder reached throughout the experiment.

that the travelling waves had a higher frequency compared to the Newtonian case, and the frequency further increased at higher elasticities. Dutcher et al. [18] reported that elastic effects in wavy flows at high Reynolds numbers ($Re \cong 800$), modified the structure of inflows and outflows. Lacassagne et al. [29] reported the sudden appearance of a dominant periodic frequency for a highly elastic and shear-thinning fluid, resembling the mode described in this work. However, unlike present findings, the observed frequency of the wavy instability mode in [29] was found to be constant, remained lower than the rotational frequency at all times and was associated with the persistence of previously existing RSW structures. The EWVF observed in the present work differs from the aforementioned ones; it appears in low Reynolds numbers at a purely Newtonian transition of a Boger fluid and alters the basic WVF without adding any additional peak on the frequency spectra. This early Hopf bifurcation is attributed to weak fluctuations caused by elastic stresses in the flow as it does not appear in the non-elastic case. Unlike Modulated Wavy Vortex Flow, in which a second frequency appears due to the modulation of the basic frequency and the instability is quasi-periodic in nature [41], the observed elastic instability is periodic, resembling WVF, but altering its characteristic frequency (Fig. 3a).

The argument that EWVF is elastic in nature is also suggested by the presence of hysteretic effects in the flow. Although the critical Reynolds number for the primary bifurcation to TVF from CF during ramp-down stays constant ($Re = 100$), the Reynolds range for the appearance of EWVF becomes smaller and is shifted to lower Re numbers ($Re = 143 - 161$) in ramp-down experiments (Fig. 4b). However, EWVF has identical spatial and temporal spectra at both ramp-up and ramp-down. Following EWVF, WVF onsets at $Re = 161$, i.e., at a critical Re lower than the equivalent for the ramp-up or the Newtonian case, signifying that the transition is subcritical. This also implies destabilization of the flow during the ramp-down by the presence of polymers even though WVF is considered a purely inertial instability.

Increasing the polymer concentration above the critical overlap concentration c^* ($El = 0.008$), does not alter the transition observed for the less elastic case, $El = 0.003$ (Fig. 5, the maps are omitted for brevity). This implies that the appearance of elastic transitions is highly dependent on the extensibility of the polymer chains [33,37] rather than the entanglement of polymer chains.

However, the critical Reynolds numbers and the Reynolds span for each regime vary with El. Both the primary and secondary bifurcation onset earlier ($Re^{ru}_{TVF} = 95$ and $Re^{ru}_{EWVF} = 140$) for $El = 0.008$, compared to the lower El transitions (Fig. 5) for the case of cylinder acceleration, in agreement with the analytical work of [43]. On the other hand, the onset of WVF is delayed ($Re^{ru}_{WVF} = 210$ for $El = 0.003$, compared to $Re_{cr} = 200$ for the Newtonian case). After this point, the elastic wavy instability is replaced by the inelastic WVF. However, the vortex pairs drift axially (Fig. 4b in the WVF regime), in contrast to the Newtonian case, illustrating the impact of the elasticity on the stability of the flow even within the WVF regime.

For a decelerating inner cylinder, WVF extends to a lower Reynolds number $Re = 133$ in the case of $El = 0.008$. Similarly, EWVF shifts to lower Reynolds numbers $Re = 121 - 133$ and persists for a smaller Re range. The lower critical Reynolds number in ramp-down compared to ramp-up are evidence of hysteretic flow behaviour.

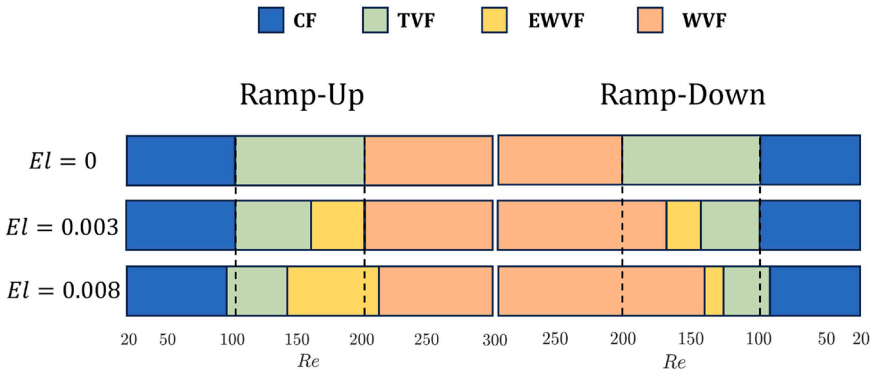

Fig. 5. Overview of the effect of Elasticity number (El) on the critical Reynolds number for flow transitions in ramp-up (left) and ramp-down (right) experiments, $El = 0 - 0.008$.

Detailed spatiotemporal maps from steady-state experiments, 1 s in duration, are illustrated in Fig. 6 for the inelastic case at TVF ($Re = 180$) and WVF ($Re = 250$). To further elucidate the nature of EWVF, maps have been produced for the two elastic cases at the same Re.

In all cases, the inflows and outflows are highlighted and noted with arrows. Outflows appear stronger for Newtonian-like fluids due to centrifugal forces [21,47]. We fit a generalized sinusoidal function $A\sin(\omega t + \varphi)$ to capture the periodicity of these boundaries (black and magenta lines in Fig. 6). In the inelastic case, inflows and outflows are stable in the TVF regime, whereas in WVF only the inflows oscillate (Fig. 6, first column). In the low elasticity fluids, both inflows and outflows oscillate in the EWVF and WVF regimes, at the same frequency. Interestingly, the oscillations are out of phase $\Delta\varphi = 2\pi/5$ (Fig. 6, second and third column).

The ratio between the oscillation amplitude of the outflows and inflows is found $A_r = A_{out}/A_{in} = 0.7$ for EWVF, independent of the fluid elasticity. This is in good agreement with ([9,10]) who reported that while in Newtonian fluids only the inflows oscillate, both inflows and outflows tend to oscillate with the same amplitude for shear-thinning fluids with increased elastic properties. The stronger inflow jet oscillations in Newtonian fluids have been attributed to the increased strength of the outflow jets [47], which hinders the axial flow between adjacent vortices.

Similarly, the oscillations of the outflow boundaries in elastic fluids can be attributed to the weakening of the outflow strength due to the opposing inward-acting elastic forces. In WVF, the amplitude ratio decreases to $A_r = 0.5$, with the amplitude of inflows remaining the same and that of outflows decreasing relative to EWVF; this is due to the outflow jets becoming stronger due to the increasing inertia, in agreement with [47]. The amplitude ratio A_r seems thus, highly dependent on the Reynolds number, decreasing as the role of inertia increases.

Although the fluid elasticity does not alter the ratio A_r, it has a strong effect on the amplitude of the oscillations of both inflows and outflows. For $El = 0.003$, the amplitude of outflows and inflows are $A_{out} = 0.07d$ and $A_{in} = 0.1d$ for EWVF, $A_{out} = 0.05d$ and $A_{in} = 0.1d$ for WVF (Table 3). For $El = 0.008$ the amplitudes are more than double these values ($A_{out} = 0.15d$ and $A_{in} = 0.22d$ for EWVF, $A_{out} = 0.11d$ and $A_{in} = 0.22d$ for WVF (Table 3). The opposite effect is reported in [14] for low-elasticity fluids, where increased elasticity leads to a decrease in the amplitude of oscillations. This can be attributed either to the significant shear-thinning of the fluids used in their study or the larger radius ratio ($\eta = 0.88$).

This increase in the amplitude of oscillations might be connected to the emergence of RSW in the case of more elastic fluids, $El > 0.01$ as reported by [4], even at much lower Re [31]. This flow state, illustrated in Fig. 7a for the high-molecular-weight fluid ($El = 0.06$) at $Re = 105$, has been previously stated to be inertia driven but modified by elasticity [39] without however making any direct connection to the Newtonian instabilities. RSW has a characteristic frequency equal to $f_{el}/3$, where $f_{el} = 2c_e/\lambda$ is the elastic wave frequency and $c_e = \sqrt{\eta/\rho t_e}$ is the wave celerity, in agreement with previously reported values in the literature [31,33]. This frequency is significantly lower than the inelastic and slightly elastic wave frequencies (Fig. 7b). The similarity of the inflows and outflows in the spatiotemporal map in Fig. 7a, implies a radial inflow/outflow symmetry as suggested by [25,26].

Fitting the generalized sinusoidal function used previously to the RSW boundaries (Fig. 7a) also reveals an inflow/outflow boundary oscillatory behavior similar to that of the wavy instabilities. However, the amplitudes of inflow and outflow oscillations are equal ($A_{out} = A_{in} = 0.22d$, $A_r = 1$) and the phase lag increases to $\Delta\varphi = \pi$ (Table 3).

On close inspection, one can observe that the waves are not perfectly sinusoidal; they are distorted every half period (Fig. 7a). At these points, momentum is transferred between adjacent vortices, allowing the propagation of the axial, elastic wave described in [31,33]. A similar mechanism is not possible at lower elasticities as (i) A_r is not equal to unity and (ii) the phase lag is significantly lower; hence the two boundaries do not approach each other.

In light of these observations, we can consider RSW an extension of the aforementioned elastically modulated wavy instabilities at the limit of high amplitude, large phase lag boundary oscillations. Since wavy instabilities are attributed to an azimuthally propagating wave [2,28,47], we postulate that RSW and its characteristic frequency should not be considered solely the result of an axial elastic wave but rather as a highly three-dimensional flow state, emerging as a combination of both an azimuthal inertial and an axial, elastic wave. Further work is however needed to fully comprehend its exact mechanism.

4. Summary

In this study, two solutions of low molecular weight PAAM have been used to elucidate the effect of very small elasticities and increasing polymer entanglement on the Newtonian transitions in Taylor Couette Flow.

It has been found that increasing polymer concentration from the dilute (1500 ppm, $c/c^* = 0.38$) to a semi-dilute (5000 ppm, $c/c^* = 1.26$) regime is not a sufficient condition for the appearance of highly elastic instabilities like RSW or FP; the extensibility of the polymer chains rather appears to be the key factor. However, a low elasticity signature, termed Elastic Wavy Vortex Flow (EWVF) has been observed for both solutions, which has not been reported in the literature hitherto. This instability was observed prior to the appearance of WVF and has similar time-dependent, single-frequency, non-axisymmetric characteristics. The characteristic feature of this new mode is the lower frequency compared to the typical WVF frequency in the Taylor-Couette system used.

Using steady-state experiments with both inelastic and elastic fluids,

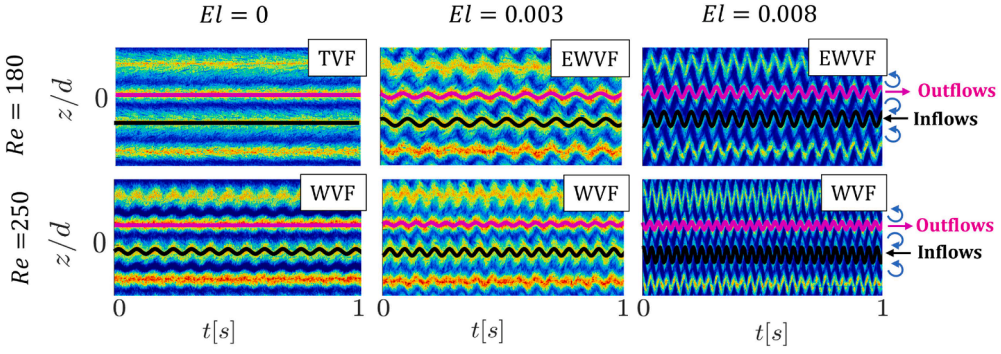

Fig. 6. Spatiotemporal maps during steady-state experiments for the inelastic case ($El = 0$) and the two elastic cases ($El = 0.003$ and $El = 0.008$) for $Re = 180$ and $Re = 250$. The sinusoidal fitting to the oscillatory inflow (black lines) and outflow regions (magenta lines) is shown in all cases. The steady-state maps capture 5 and 9 ($El = 0$), 8 and 15 ($El = 0.003$), 15 and 21 ($El = 0.008$) revolutions of the inner cylinder at $Re = 180$ and $Re = 250$ respectively.

Table 3
Amplitude characteristics of the oscillating outflow and inflow boundaries (A_{out}, A_{in}) for El = 0 - 0.06

	RSW (Re = 105)			EWVF (Re = 180)			WVF(Re = 250)		
El	A_{in}/d	A_{out}/d	A_r	A_{in}/d	A_{out}/d	A_r	A_{in}/d	A_{out}/d	A_r
0	–			–			0.07	0	0
0.003	–			0.10	0.07	0.7	0.10	0.05	0.5
0.008	–			0.22	0.15	0.7	0.22	0.11	0.5
0.06	0.22	0.22	1	–			–		

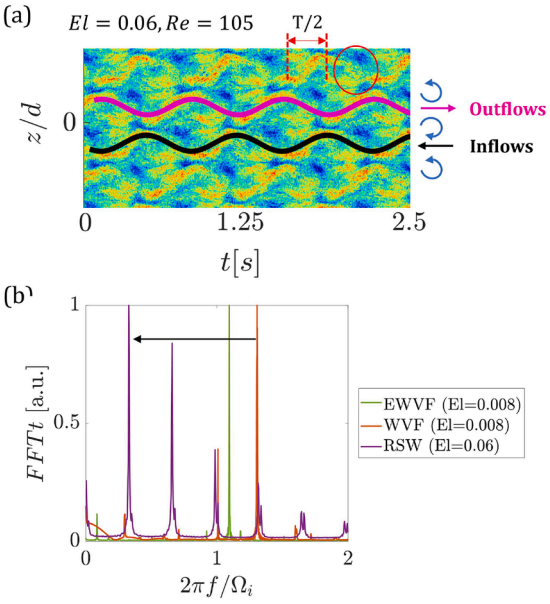

Fig. 7. (a) Steady-state spatiotemporal map of Rotating Standing Waves (RSW) for a polymeric fluid with $El = 0.06$ at $Re = 105$. Sinusoidal fits to the oscillating inflow (black lines) and outflow regions (magenta lines) are superimposed. (b) Temporal spectra of the RSW in comparison with wavy instabilities ($Re = 180$ - TVF, $Re = 250$ - WVF) for a less elastic solution ($El = 0.008$).

we concluded that (i) the value of El (and thus here the entanglement state) modifies the frequency of the additional EWVF state, but (ii) the frequency of WVF is not altered, only its structure.

The waviness appears on both outflow and inflow boundaries as described by ([9,10]) and can thus, be attributed to elasticity and not the shear-thinning nature of the fluids used in their study.

For increasing elasticity, the Re range at which TVF is observed decreases while for EWVF increases during ramp-up. At the same time, WVF is delayed (appears at higher Reynolds number). For ramp-down, a slightly hysteretic behaviour is observed as all flow states are sustained to lower Re.

By fitting a sinusoidal function to the wavy oscillations, we conclude that increased elasticity leads to an increase in the amplitude of oscillations of both inflow and outflow boundaries. This effect along with the increase in the phase lag of the two oscillating boundaries, potentially links the elastic RSW flow state to the Newtonian-like instabilities.

The present study highlights the importance of elastic phenomena on flow transitions and provides evidence that the additions of even small amounts of polymers may enhance the intercellular mixing, as both inflow and outflow boundaries oscillate, even at Re lower than the inelastic Newtonian case. However, caution may be exercised on the use of low molecular weight polymers to increase the viscosity of fluids, which is a common technique [15,34,35], as they can potentially induce undesirable elastic instabilities. In addition, considering RSW as an extension of the wavy instabilities may bear significant changes to our understanding of the phenomenon as both an axial and an azimuthal wave may contribute to its mechanism.

CRediT authorship contribution statement

T. Boulafentis: Writing – original draft, Visualization, Methodology, Investigation, Data curation. **T. Lacassagne:** Writing – review & editing, Visualization, Methodology, Investigation, Data curation. **N. Cagney:** Writing – review & editing, Visualization, Methodology, Investigation, Data curation. **S. Balabani:** Writing – review & editing, Supervision, Resources, Funding acquisition, Conceptualization.

Declaration of competing interest

The authors declare that they have no known competing financial interests or personal relationships that could have appeared to influence the work reported in this paper.

Data availability

Data will be made available on request.

Funding

Financial support for this work from the Engineering and Physical Sciences Research Council (EPSRC) Manufacturing the Future programme (grant no. EP/N024915/1) as well as the EPSRC DTP award EP/R513143/1 is gratefully acknowledged.

References

[1] A. Akonur, R.M. Lueptow, Chaotic mixing and transport in wavy Taylor–couette flow, Phys. D: Nonlinear Phenom. 167 (3–4) (2002) 183–196, https://doi.org/10.1016/S0167-2789(02)00529-8.
[2] A. Akonur, R.M. Lueptow, Three-dimensional velocity field for wavy Taylor–couette flow, Phys. Fluids 15 (4) (2003) 947–960, https://doi.org/10.1063/1.1556615.
[3] C.D. Andereck, S.S. Liu, H.L. Swinney, Flow regimes in a circular couette system with independently rotating cylinders, J. Fluid. Mech. 164 (1986) 155–183, https://doi.org/10.1017/S0022112086002513.
[4] M. Avgousti, A.N. Beris, Non-axisymmetric modes in viscoelastic Taylor-Couette flow, J. Nonnewton Fluid Mech. 50 (2–3) (1993) 225–251, https://doi.org/10.1016/0377-0257(93)80033-8.
[5] B.M. Baumert, S.J. Muller, Flow visualization of the elastic Taylor-Couette instability in boger fluids, Rheol. Acta. 34 (2) (1995) 147–159, https://doi.org/10.1007/BF00398434.
[6] D.W. Beard, M.H. Davies, K. Walters, The stability of elastico-viscous flow between rotating cylinders Part 3. overstability in viscous and maxwell fluids, J. Fluid Mech. 24 (2) (1966) 321–334, https://doi.org/10.1017/S0022112066000673.
[7] T. Boulafentis, T. Lacassagne, N. Cagney, S. Balabani, Experimental insights into elasto-inertial transitions in Taylor–Couette flows, Philos. Trans. R. Soc. A: Math. Phys. Eng. Sci. (2243) (2023) 381, https://doi.org/10.1098/rsta.2022.0131.
[8] M.G. Brereton, Dynamics of Polymeric Liquids, Phys. Bull. 29 (1) (1978) 26, https://doi.org/10.1088/0031-9112/29/1/038.
[9] N. Cagney, S. Balabani, Taylor-Couette flow of shear-thinning fluids, Phys. Fluids 31 (5) (2019) 053102, https://doi.org/10.1063/1.5088143.
[10] N. Cagney, S. Balabani, Influence of shear-thinning rheology on the mixing dynamics in Taylor-Couette flow, Chem. Eng. Technol. 42 (8) (2019) 1680–1690, https://doi.org/10.1002/ceat.201900015.
[11] N. Cagney, T. Lacassagne, S. Balabani, Taylor–Couette flow of polymer solutions with shear-thinning and viscoelastic rheology, J. Fluid. Mech. 905 (2020) A28, https://doi.org/10.1017/jfm.2020.701.
[12] L. Campo-Deaño, C. Clasen, The slow retraction method (SRM) for the determination of ultra-short relaxation times in capillary breakup extensional

rheometry experiments, J. Nonnewton. Fluid. Mech. 165 (23–24) (2010) 1688–1699, https://doi.org/10.1016/j.jnnfm.2010.09.007.
[13] K.T. Coughlin, P.S. Marcus, Modulated waves in Taylor-Couette flow Part 1. Analysis, J. Fluid. Mech. 234 (1) (1992) 1, https://doi.org/10.1017/S0022112092000673.
[14] O. Crumeyrolle, I. Mutabazi, M. Grisel, Experimental study of inertioelastic Couette–Taylor instability modes in dilute and semidilute polymer solutions, Phys. Fluids 14 (5) (2002) 1681–1688, https://doi.org/10.1063/1.1466837.
[15] M. Davoodi, S. Lerouge, M. Norouzi, R.J. Poole, Secondary flows due to finite aspect ratio in inertialess viscoelastic Taylor–Couette flow, J. Fluid. Mech. 857 (2018) 823–850, https://doi.org/10.1017/jfm.2018.746.
[16] J. Dusting, S. Balabani, Mixing in a Taylor–Couette reactor in the non-wavy flow regime, Chem. Eng. Sci. 64 (13) (2009) 3103–3111, https://doi.org/10.1016/j.ces.2009.03.046.
[17] C.S. Dutcher, S.J. Muller, Spatio-temporal mode dynamics and higher order transitions in high aspect ratio Newtonian Taylor–Couette flows, J. Fluid. Mech. 641 (2009) 85–113, https://doi.org/10.1017/S0022112009991431.
[18] C.S. Dutcher, S.J. Muller, Effects of weak elasticity on the stability of high Reynolds number co- and counter-rotating Taylor-Couette flows, J. Rheol. (N. Y. N. Y) 55 (6) (2011) 1271–1295, https://doi.org/10.1122/1.3626584.
[19] H. Elçiçek, B. Güzel, Effect of shear-thinning behavior on flow regimes in Taylor–Couette flows, J. Nonnewton. Fluid. Mech. 279 (279) (2020) 104277, https://doi.org/10.1016/j.jnnfm.2020.104277.
[20] M.P. Escudier, I.W. Gouldson, D.M. Jones, Taylor vortices in Newtonian and shear-thinning liquids, Proceedings of the Royal Society of London. Series A: Mathematical and Physical Sciences 449 (1935) (1995) 155–176, https://doi.org/10.1098/rspa.1995.0037.
[21] M.A. Fardin, C. Perge, N. Taberlet, The hydrogen atom of fluid dynamics" – introduction to the Taylor–Couette flow for soft matter scientists, Soft. Matter. 10 (20) (2014) 3523, https://doi.org/10.1039/c3sm52828f.
[22] P.R. Fenstermacher, H.L. Swinney, J.P. Gollub, Dynamical instabilities and the transition to chaotic Taylor vortex flow, J. Fluid. Mech. 94 (1) (1979) 103–128, https://doi.org/10.1017/S0022112079000963.
[23] J.J.J. Gillissen, N. Cagney, T. Lacassagne, A. Papadopoulou, S. Balabani, H. J. Wilson, Taylor-Couette instability in disk suspensions: experimental observation and theory, Phys. Rev. Fluids. 5 (8) (2020) 083302, https://doi.org/10.1103/PhysRevFluids.5.083302.
[24] M. Gorman, H.L. Swinney, Spatial and temporal characteristics of modulated waves in the circular Couette system, J. Fluid. Mech. 117 (1982) 123–142, https://doi.org/10.1017/S0022112082001554.
[25] A. Groisman, V. Steinberg, Solitary vortex pairs in viscoelastic couette flow, Phys. Rev. Lett. 78 (8) (1997) 1460–1463, https://doi.org/10.1103/PhysRevLett.78.1460.
[26] A. Groisman, V. Steinberg, Mechanism of elastic instability in couette flow of polymer solutions: experiment, Phys. Fluids 10 (10) (1998) 2451–2463, https://doi.org/10.1063/1.869764.
[27] E. Imomoh, J. Dusting, S. Balabani, On the quasiperiodic state in a moderate aspect ratio taylor–couette flow, Phys. Fluids 22 (4) (2010) 1–10, https://doi.org/10.1063/1.3407665.
[28] G.P. King, Y. Lee, W. Li, H.L. Swinney, P.S. Marcus, Wave speeds in wavy Taylor-vortex flow, J. Fluid. Mech. 141 (1984) 365–390, https://doi.org/10.1017/S0022112084000896.
[29] T. Lacassagne, T. Boulafentis, N. Cagney, S. Balabani, Modulation of elasto-inertial transitions in Taylor–Couette flow by small particles, J. Fluid. Mech. 929 (2021) R2, https://doi.org/10.1017/jfm.2021.861.
[30] T. Lacassagne, N. Cagney, S. Balabani, Shear-thinning mediation of elasto-inertial Taylor–Couette flow, J. Fluid. Mech. 915 (2021) A91, https://doi.org/10.1017/jfm.2021.104.
[31] T. Lacassagne, N. Cagney, J.J.J. Gillissen, S. Balabani, Vortex merging and splitting: a route to elastoinertial turbulence in Taylor-Couette flow, Phys. Rev. Fluids. 5 (11) (2020) 113303, https://doi.org/10.1103/PhysRevFluids.5.113303.
[32] N. Latrache, N. Abcha, O. Crumeyrolle, I. Mutabazi, Defect-mediated turbulence in ribbons of viscoelastic Taylor-Couette flow, Phys. Rev. E 93 (4) (2016) 043126, https://doi.org/10.1103/PhysRevE.93.043126.
[33] J.M. Lopez, Vortex merging and splitting events in viscoelastic Taylor–Couette flow, J. Fluid. Mech. 946 (2022) A27, https://doi.org/10.1017/jfm.2022.579.
[34] B. Martínez-Arias, J. Peixinho, Torque in Taylor–Couette flow of viscoelastic polymer solutions, J. Nonnewton. Fluid. Mech. 247 (2017) 221–228, https://doi.org/10.1016/j.jnnfm.2017.07.005.
[35] S. Migliozzi, L. Mazzei, P. Angeli, Viscoelastic flow instabilities in static mixers: onset and effect on the mixing efficiency, Physics of Fluids 33 (1) (2021), https://doi.org/10.1063/5.0038602.
[36] D.G. Satchwell, T. Mullin, Bifurcation phenomena in Taylor—Couette flow of elastic polymer solutions, Proc.R. Soc. Lond. Series A: Math. Phys. Eng. 457 (2015) (2001) 2567–2583, https://doi.org/10.1098/rspa.2001.0837.
[37] J. Song, F. Lin, N. Liu, X.-Y. Lu, B. Khomami, Direct numerical simulation of inertio-elastic turbulent Taylor–Couette flow, J. Fluid. Mech. 926 (2021) A37, https://doi.org/10.1017/jfm.2021.757.
[38] P.C. Sousa, E.J. Vega, R.G. Sousa, J.M. Montanero, M.A. Alves, Measurement of relaxation times in extensional flow of weakly viscoelastic polymer solutions, Rheol. Acta 56 (1) (2017) 11–20, https://doi.org/10.1007/s00397-016-0980-1.
[39] V. Steinberg, A. Groisman, Elastic versus inertial instability in Couette-Taylor flow of a polymer solution, Review. Phil. Mag. B 78 (2) (1998) 253–263, https://doi.org/10.1080/13642819808202948.
[40] Y. Takeda, Quasi-periodic state and transition to turbulence in a rotating Couette system, J. Fluid. Mech. 389 (1999) 81–99, https://doi.org/10.1017/S0022112099005091.
[41] Y. Takeda, W.E. Fischer, K. Kobashi, T. Takada, Spatial characteristics of dynamic properties of modulated wavy vortex flow in a rotating Couette system, Exp. Fluids. 13 (2–3) (1992) 199–207, https://doi.org/10.1007/BF00218167.
[42] G.I. Taylor, VIII. Stability of a viscous liquid contained between two rotating cylinders, Philos. Trans. R. Soc. London. Series A, Containing Papers of a Mathematical or Physical Character 223 (605–615) (1923) 289–343, https://doi.org/10.1098/rsta.1923.0008.
[43] R.H. Thomas, K. Walters, The stability of elastico-viscous flow between rotating cylinders, Part 1. J. Fluid. Mech. 18 (1) (1964) 33–43, https://doi.org/10.1017/S0022112064000039.
[44] R.H. Thomas, K. Walters, The stability of elastico-viscous flow between rotating cylinders. Part 2, J. Fluid. Mech. 19 (4) (1964) 557–560, https://doi.org/10.1017/S002211206400091X.
[45] S. Topayev, C. Nouar, D. Bernardin, A. Neveu, S.A. Bahrani, Taylor-vortex flow in shear-thinning fluids, Phys. Rev. E 100 (2) (2019) 023117, https://doi.org/10.1103/PhysRevE.100.023117.
[46] K. Watanabe, S. Sumio, S. Ogata, Formation of taylor vortex flow of polymer solutions, J. Fluids. Eng. 128 (1) (2006) 95–100, https://doi.org/10.1115/1.2137350.
[47] S.T. Wereley, R.M. Lueptow, Spatio-temporal character of non-wavy and wavy Taylor–Couette flow, J. Fluid. Mech. 364 (1998) 59–80, https://doi.org/10.1017/S0022112098008969.
[48] S. Topayev, C. Nouar, J. Dusek, Secondary instabilities in Taylor–Couette flow of shear-thinning fluids, J. Fluid Mech. 933 (2022) A4, https://doi.org/10.1017/jfm.2021.1036.